

## **Pressure Induced Superconductivity in the New Compound $\text{ScZrCo}_{1-6}$**

Enyu Wang<sup>\*</sup>, Jing Si<sup>\*</sup>, Xiyu Zhu<sup>†</sup>, Guan-Yu Chen, Hai Lin & Hai-Hu Wen<sup>†</sup>

Center for Superconducting Physics and Materials, National Laboratory of Solid State  
Microstructures and Department of Physics, Collaborative Innovation Center for  
Advanced Microstructures, Nanjing University, Nanjing 210093, China

<sup>\*</sup>These authors contributed equally to this work.

**It is widely perceived that the correlation effect may play an important role in several unconventional superconducting families, such as cuprate, iron-based and heavy-fermion superconductors. The application of high pressure can tune the ground state properties and balance the localization and itineracy of electrons in correlated systems, which may trigger unconventional superconductivity. Moreover, non-centrosymmetric structure may induce the spin triplet pairing which is very rare in nature. Here, we report a new compound  $\text{ScZrCo}_{1-6}$  crystallizing in the  $\text{Ti}_2\text{Ni}$  structure with the space group of  $FD3-MS$  without a spatial inversion center. The resistivity of the material at ambient pressure shows a bad metal and weak semiconducting behavior. Furthermore, specific heat and magnetic susceptibility measurements yield a rather large value of Wilson ratio  $\sim 4.47$ . Both suggest a ground state with correlation effect. By applying pressure, the up-going behavior of**

resistivity in lowering temperature at ambient pressure is suppressed and gradually it becomes metallic. At a pressure of about 19.5 GPa superconductivity emerges. Up to 36.05 GPa, a superconducting transition at about 3.6 K with a quite high upper critical field is observed. Our discovery here provides a new platform for investigating the relationship between correlation effect and superconductivity.

## Introduction

The discoveries of superconductivity in cuprate<sup>1-2</sup> and iron-pnictides / chalcogenides<sup>3-5</sup> have revived the enthusiasm of exploring new high temperature superconductors in correlated systems. It is known that both copper and iron in these families are *3d* transition metal elements. In many compounds containing *3d* transition metal elements, the strong interaction of electrons cannot be neglected leading to a correlation effect and subtle balance between localization and itinerancy of *d*-orbital electrons<sup>6</sup>. And this correlation effect induces tremendous and rich physics, including unconventional superconductivity<sup>7</sup>, Mott insulating state<sup>8</sup>, bad metal, spin density wave, etc.<sup>9,10</sup>. By doping charge carriers or applying external pressure, the correlation effect can be tuned and the ordering states are suppressed, thus triggering possible superconductivity. Following this idea, superconductivity has been found in  $\text{Na}_x\text{CoO}_2 \cdot 1.3\text{H}_2\text{O}$ <sup>11</sup>,  $\text{MnP}$ <sup>12</sup>,  $\text{CrAs}$ <sup>13</sup>,  $\text{Ba}_{1-x}\text{Na}_x\text{Ti}_2\text{Sb}_2\text{O}$ <sup>14,15</sup>, etc.. Therefore, it is a promising way to explore unconventional superconductivity in compounds with *3d* transition metal elements.

As cobalt is a typical *3d* transition metal element and lies between iron and copper,

the superconductors containing cobalt are generally interesting and unusual. Superconductors containing Co include compounds such as CeCoIn<sub>5</sub>, Na<sub>x</sub>CoO<sub>2</sub>·1.3H<sub>2</sub>O and Zr<sub>2</sub>Co. CeCoIn<sub>5</sub> is a well-known unconventional heavy-fermion superconductor<sup>16</sup> with  $T_c = 2.3$  K. And the superconductor Na<sub>x</sub>CoO<sub>2</sub>·1.3H<sub>2</sub>O with  $T_c \approx 4$  K is fascinating for its strong electron correlation effect, which may have a *d*-wave gap symmetry reflecting unconventional superconducting pairing mechanisms<sup>17</sup>. In the cobaltite Na<sub>0.7</sub>CoO<sub>2</sub>, a Curie-Weiss metallic phase was reported, which was argued to be induced by correlation effect<sup>18, 19</sup>. The cobalt alloy Zr<sub>2</sub>Co, which crystalizes in the CuAl<sub>2</sub> structure (space group: *I4/MCM*) was also reported as a superconductor with  $T_c = 5$  K<sup>20</sup>. And the NMR investigation revealed that it could be an itinerant antiferromagnet in the normal state<sup>21</sup>. Here, we report the discovery of a new compound ScZrCo<sub>1-δ</sub> with a non-centrosymmetric structure. It does not crystalize in the tetragonal CuAl<sub>2</sub> structure but in the cubic Ti<sub>2</sub>Ni structure with the space group *FD3-MS*<sup>22</sup>. An anomalous ground state is found and superconductivity is induced by pressurizing the material to a high pressure.

## Results

**Characterization of the crystal structure and composition.** Fig. 1a shows the X-ray diffraction patterns for the sample ScZrCo<sub>1-δ</sub> and the Rietveld fitting curve (the red line) to the data<sup>23</sup>. The Rietveld refinement gives a quite good agreement between the measured data and the calculated profile with the agreement factor  $R_{WP} = 1.551$  %. And no obvious impurity peaks are found. The lattice parameters for the

cubic unit cell are determined to be  $a = b = c = 12.22 \text{ \AA}$ . The inset shows the schematic structure of  $\text{ScZrCo}_{1-\delta}$  with the space group  $FD3-MS$ . And as shown in Table 1, there are two sites for Sc and Zr, which are occupied by Sc and Zr atoms in approximately the 1:1 ratio. And the occupancies of each site for Sc and Zr are given in Table 1, this is obtained by the best Rietveld fit ( $R_{WP} = 1.551\%$ ). Apparently, all Co atoms occupy the same site, and every four nearest Co atoms form a tetrahedron, with a Co-Co bond with length of  $3.043 \text{ \AA}$ . This tetrahedron is surrounded by Sc and Zr atoms. Every tetrahedron together with other four nearest tetrahedron assembles a larger tetrahedron. Thus, there is no spatial inversion symmetry in this compound. Fig. 1b shows a representative energy dispersive X-ray spectrum (EDS) of a micro area on our  $\text{ScZrCo}_{1-\delta}$  polycrystalline sample. The SEM photograph of the sample is shown in the right upper position of Fig. 1b, while the element ratio in this area is very close to 1: 1: 1. To estimate the accurate ratio of the compound, we have detected the compositions in eight areas on three samples. They are quite close to each other. The averaged ratio among the compositions Sc: Zr: Co is 1.00: 1.09: 0.91. It seems that the Co has a slight deficiency, which may be substituted by the extra Zr.

**Magnetic susceptibility and specific heat.** The temperature dependence of magnetic susceptibility is shown in Fig. 2a with an applied magnetic field of 1 T. There is a small hump at about 50 K, which is caused by the antiferromagnetic transition of frozen oxygen. Since this phenomenon appears quite often in our SQUID and is irrelevant to the related physics here, we have already removed this hump by using a wave packet

of Gaussian function. Using the Curie-Weiss law, we fit the data by the equation  $\chi(T) = c/(T+T_0) + \chi(0)[1-(T/T_E)^2]$ . The first term of the equation arises from the local magnetic moments of the ions at paramagnetic sites, and the second one is the Pauli paramagnetic susceptibility term which is related to the quasiparticle density of states (DOS) at Fermi level<sup>24, 25</sup>. The fitting yields  $c = 0.0013$  emu K/mol Oe,  $T_0 = 0.8$  K,  $\chi(0) = 0.0006$  emu/mol Oe,  $T_E = 1295.7$  K. As for  $c = \mu_0 \mu_{eff}^2 / 3k_B$ , the effective magnetic moment per Co can be estimated to be around  $0.10\mu_B$ . In Fig. 2b, we present the specific heat coefficient  $C/T$  vs.  $T^2$ . As shown in the inset, in the low temperature region ( $T < 10$  K), we fit the experimental data with the Debye model  $C/T = \gamma_n + \beta T^2$  and  $\beta = 12\pi^4 N_A Z k_B T^2 / 5\Theta_D^3$ . Using the value of Avogadro constant  $N_A = 6.02 \times 10^{23}$  mol<sup>-1</sup>, Boltzmann constant  $k_B = 1.38 \times 10^{-23}$  J/K,  $Z = 3$  (the number of atoms in a primitive cell), the Debye temperature  $\Theta_D$  is estimated to be 248.7 K. In contrast to the Debye model fitting as shown by the red line here, there is a slight but clear upturn for the data in the low temperature limit. This upturn may be induced by the Schottky anomaly or the correlation effect. However its smooth temperature dependent evolution together with the large Wilson ratio may exclude the former case. The low temperature upturning of specific heat coefficient and deviation from the Debye model fitting suggests the presence of correlation effect. A polynomial fitting to the data in the low temperature limit gives  $\gamma_n = 9.75$  mJ/mol K<sup>2</sup>.

**Temperature dependence of resistivity under high pressure.** The temperature dependence of resistivity for ScZrCo<sub>1- $\delta$</sub>  at various pressures is presented in Fig. 3a. At

ambient pressure, the resistivity curve exhibits a rising upon lowering temperature in the whole temperature region from 1.9 K to 300 K, which reveals a bad metal or weak semiconducting behavior. The temperature dependence of resistivity cannot be fitted with the model  $\rho = \rho_0 \exp[-k_B T / E_g]$  with a band gap  $E_g$ . By applying pressure, the resistivity reduces gradually, and the up-going behavior at ambient pressure is suppressed, transforming to a metallic one. As the pressure reaches 19.05 GPa, the superconductivity shows up above 1.9 K with a small but sharp upturning in low temperature region, which may result from the non-standard four-point measurement and the superconducting current passes through a zig-zag way. This upturn can also be suppressed with increasing magnetic field. For this reason we regard the onset transition temperature as the point where this upturn starts. As we increase the pressure further, the superconducting transition temperature gets increased. At 36.05 GPa, the highest pressure we can reach in this run of experiment, superconductivity with an onset transition temperature  $T_c = 3.6$  K has been observed, and meanwhile the zero resistivity is also observed at a lower temperature. Fig. 3b shows the normalized resistivity. As we can see, the value of residual-resistivity-ratio ( $RRR$ ) drops gradually with the pressure below 24.51 GPa. Then, the  $RRR \approx 1.26$  keeps almost unchanged with further increasing the pressure up to 36.05 GPa. The inset of Fig. 3b shows the enlarged view of the low temperature resistivity at 16.26 GPa and 36.05 GPa.

**Phase diagram for  $T_c$ - $P$  and  $\rho_{4K}/\rho_{300K}$ - $P$ .** To determine the superconducting critical

transition temperature, we have adopted different criterions: the onset superconducting transition temperature  $T_c^{\text{onset}}$  is determined from the very beginning of the deviating point of the normal state resistivity curve; the critical temperatures with  $50\%\rho_{4K}$  and  $90\%\rho_{4K}$ , where  $\rho_{4K}$  is the resistivity at 4K. In Fig.4 we present a phase diagram which reveals the doping dependence of the superconducting transition temperature  $T_c$  and the ratio  $\rho_{4K}/\rho_{300K}$ . As shown in the phase diagram, the value of  $\rho_{4K}/\rho_{300K}$  is suppressed gradually when the pressure is increased up to 19.5 GPa. At the pressure of about 19.5 GPa, we observe a deviation of resistivity from the normal state background, which as explained above, is due to the presence of superconductivity. The superconducting transition temperature increases gradually by applying higher pressures and  $T_c$  goes up to 3.6 K under a pressure of about 36.05 GPa. The transition temperature is expected to rise further under higher pressures. From Fig.3b, we find another interesting phenomenon that when the weak semiconducting behavior is suppressed, superconductivity starts to emerge. This can easily get a reflection from the phase diagram shown in Fig.4. This set of data manifest that superconductivity shows as a subtle balance between the localization and itinerancy of electrons<sup>7</sup>.

**Upper critical field.** In Fig. 5, we present the low temperature resistivity under different magnetic fields up to 4 T at 36.05 GPa. The systematic evolution of resistivity curve under a magnetic field tells no doubt that the drop of resistivity at around 3 K is due to superconductivity. We thus determine the upper critical field  $H_{c2}$

versus temperature and display the data in the inset of Fig. 5. Here, we use the criterions of  $90\% \rho(4\text{K})$  and  $50\% \rho(4\text{K})$  to determine the value of  $H_{c2}(T)$ . From the curve with a criterion of  $90\% \rho(4\text{K})$ , we have  $-dH_{c2}/dT|_{T_c} = 2.7 \text{ T/K}$ . We further fit the  $H_{c2}$  curve with an empirical formula  $H_{c2}(T) = H_{c2}(0)[1 - (T/T_c)^2]^a [1 + (T/T_c)^2]^b$ . The fitting curve is shown by the red dashed line. For the criterion of  $90\% \rho_{4\text{K}}$ , The parameters of  $a$  and  $b$  used in the fitting are 0.74 and -0.68, respectively. The estimated  $H_{c2}(0)$  is about 5.14 T. Considering the  $T_c(90\% \rho_n)$  is 2.7 K, and the ratio of  $H_{c2}(0)/T_c = 1.9 \text{ T/K}$ .

## Discussion

**Crystal structure and inversion symmetry broken in ScZrCo<sub>1-δ</sub>.** From the Rietveld fitting, the space group of ScZrCo<sub>1-δ</sub> is determined to be *FD3-MS*, in which no inversion center can be found. Four nearest Co atoms in ScZrCo<sub>1-δ</sub> form a regular tetrahedron as shown in Fig. 1a. And five Co tetrahedrons, as four vertexes and one centroid, assemble a bigger tetrahedron. As we know, this kind of tetrahedron has a typical non-centrosymmetric geometric structure. Compounds with non-centrosymmetric structure usually behave in a unique way, especially about their superconducting order parameter. Recently, unconventional superconducting properties were observed in the non-centrosymmetric compounds CePt<sub>3</sub>Si<sup>26</sup> and Li<sub>2</sub>Pt<sub>3</sub>B<sup>27</sup> for the possible existence of spin-triplet pairing symmetry. It is curious to know whether our present system has the spin triplet pairing or not.



**Correlation effect.** The temperature dependence of magnetization at ambient pressure can be well described by the Curie-Weiss law, yielding an average magnetic moment  $\mu_{eff} \approx 0.10\mu_B/\text{Co}$ . It is very similar to the  $\text{Na}_{0.7}\text{CoO}_2$ , which also shows a Curie-Weiss law behavior and was argued to be induced by correlation effect<sup>18,19</sup>. Specific heat measurements in  $\text{ScZrCo}_{1-\delta}$  indicate that the low temperature data deviates from the Debye model and exhibit a slight upturn in the low-temperature limit, which may demonstrate the possible correlation effect in our sample. Usually the Wilson ratio can be used to determine whether there is correlation effect in the system. By definition the Wilson ratio is expressed in the form<sup>28</sup> of  $R = [4\pi^2 k_B^2 / 3(g\mu_B)^2] \chi(0) / \gamma_n$ . Here the  $k_B$  is Boltzmann constant,  $g$  is Lande factor which is 2 for a bare electron, and  $\mu_B$  is the Bohr magneton. If  $R \approx 1$ , the material is considered to be the non-interacting electron gas. If  $R$  is less than 2 but larger than 1, it corresponds to an interacting Fermi liquid. A strong electron correlation effect would be expected, if the Wilson ratio  $R > 2$ . For the present compound  $\text{ScZrCo}_{1-\delta}$ ,  $R$  is determined to be 4.47, which suggests possible strong electron correlation in the compound. In correlated systems, the localization and itinerancy is subtly balanced and the ground state can vary from a Mott insulator to an itinerant metal<sup>7</sup>. High pressure can tune the properties, which may trigger unconventional superconductivity.

**Bad metal behavior.** At ambient pressure, the resistivity curve behaves in a way of weak semiconducting, which is similar to some alloy materials such as  $\text{Ti}_{67}\text{Al}_{33}$

(Ref.29). With increasing pressure, the resistivity curve turns to a metallic behavior, but there is still a slight upturn in low temperature region. Large resistivity scale and absence of saturation in low temperature region are the typical characteristics of a bad metal. There are mainly two criterions to judge whether the resistivity scale is large or not: Ioffe-Regal limit<sup>30</sup>  $lk_F^{-1} \approx 1$ , or Mooij limit<sup>31</sup>  $\rho > 0.15 \text{ m}\Omega \text{ cm}$ . Here  $l$  is electron mean free path,  $k_F$  is Fermi wave vector. The normal state resistivity of  $\text{ScZrCo}_{1-\delta}$  at 0 GPa is above 0.88 m $\Omega$  cm. Even at the highest pressure 36.05 GPa, it is still larger than the Mooij limit. Therefore we are confident that the system is a typical bad metal caused probably by the correlation effect.

**Superconductivity at high pressure.** By applying high pressure, we have successfully tuned the ground state and induced the superconductivity above 19.5 GPa. The superconductivity emerges just after the rapid drop of normalized resistivity which is shown in Fig. 4. And the superconducting transition temperature  $T_c^{onset}$  gets to 3.6 K at 36.05 GPa. At this pressure, we obtain the upper critical field  $H_{c2} = 5.14 \text{ T}$  with the  $T_c(90\% \rho_n) = 2.72 \text{ K}$  (see the green dots in the inset of Fig. 5.). In the weak-coupling limit for a BCS superconductor, the upper critical field due to the pair breaking of Pauli limit is  $H_p [\text{T}] = 1.84 T_c [\text{K}]$ <sup>32</sup>, which corresponds to be 5.0 T for the  $\text{ScZrCo}_{1-\delta}$ .

In conclusion, we have discovered a new compound  $\text{ScZrCo}_{1-\delta}$  which has a cubic structure with the space group  $FD3-MS$  without a spatial inversion center. The ground state of this material is a bad metal showing a strange weak semiconducting

behavior. By applying pressure beyond 19.5 GPa, the system becomes superconductive. A superconducting transition temperature at about 3.6 K can be observed under 36.05 GPa. The upturning of low temperature specific heat coefficient and large Wilson ratio suggest a ground state with correlation effect. This material provides a typical platform for achieving superconductivity by finely tuning the subtle balance between localization and itinerancy of *d*-orbital electrons.

## Methods

**Sample preparation and characterization.** The polycrystalline ScZrCo<sub>1-δ</sub> samples were fabricated by the arc-melting method. The raw materials scandium (Alfa Aesar, powder, purity 99.8%), zirconium (Aladdin, powder, purity 99.9%) and cobalt (Alfa Aesar, powder, purity 99.99%) were weighed in the mole proportion 1: 1: 0.9, mixed well, and pressed into a pellet in a glove box filled with argon (water moisture and the oxygen compositions in the glove box were both below 0.1 PPM). The pellets were put on the copper base of the Arc furnace filled with argon atmosphere. To ensure the homogeneity of the samples, we re-melted the pellets by turning up and down at least 5 times. Finally, we got the silver-shining polycrystalline samples. The Bruker D8 Advance diffractometer (Cu-K<sub>α</sub> radiation) was used to measure the X-ray diffraction pattern. The energy dispersive X-ray microanalysis spectrum and the SEM photograph of the polycrystalline were obtained by S-3400NII (Hitachi). The SEM measurements were performed at an accelerating voltage of 20 kV and working distance of about 10 mm.

**Transport and magnetic measurement at ambient pressure.** The DC magnetization measurements were performed with a SQUID-VSM-7T (Quantum Design). The specific heat of a high quality ScZrCo<sub>1-δ</sub> polycrystalline. To ensure the good thermal conduction, we polish one side of the ScZrCo<sub>1-δ</sub> sample well and paste with the thermal conduction grease. The specific heat was measured by the thermal-relaxation method with the PPMS-16T (Quantum Design) which allows us to realize high vacuum atmosphere for the sample and measure its specific heat down to 2 K.

**High pressure resistivity measurements.** The measurements under high pressure were accomplished by using the diamond based system cryoDAC-PPMS (Almax easyLab). The culet size of diamonds is 400 μm. The gasket is made by T301 stainless steel which was insulated by the cubic-BN-epoxy mixture, and a small piece of ruby was used as a pressure manometer. The relation of pressure and ruby R(1) fluorescent peak is calculated by the equation  $P(\text{GPa}) = 380.8[(\Delta\lambda/\lambda_0+1)^5-1]$ <sup>33</sup>. Here  $\lambda_0$  is the position of ruby R(1) fluorescent peak at ambient pressure. And  $\Delta\lambda = \lambda - \lambda_0$  ( $\lambda$  is the position of ruby R(1) fluorescent peak at the pressure  $P$ .) The hole size of the gasket is 200 μm. The pressure transmitting medium was the ScZrCo<sub>1-δ</sub> polycrystalline powder itself. Then we used the PPMS-9T (Quantum Design) to measure the temperature-dependent resistivity.

## Acknowledgements

We acknowledge the useful discussions with Xiangang Wang and Igor Mazin. This work was supported by the Ministry of Science and Technology of China (Grant No. 2016YFA0300401, 2016YFA0401700), and the National Science Foundation China (NSFC) with the projects: A0402/11534005, A0402/11674164, E0211/51302133.

## Author contributions

The high pressure resistivity measurements were finished by EYW and JS. The samples were synthesized by JS and XYZ. The specific heat measurements were finished by GYC, and magnetization at ambient pressure measurements were finished by EYW, JS and HL. The data analysis was done by EYW, SJ, XYZ and HHW. HHW coordinated the whole work. EYW, XYZ and HHW wrote the manuscript. All authors have discussed the results and the interpretation.

## Competing financial interests

The authors declare that they have no competing financial interests.

\* Correspondence and requests for materials should be addressed to

[zhuxiyu@nju.edu.cn](mailto:zhuxiyu@nju.edu.cn), [hhwen@nju.edu.cn](mailto:hhwen@nju.edu.cn).

## References

1. Bednorz, J. G. & Müller, K. A. Possible high  $T_c$  superconductivity in the Ba-La-Cu-O system. *Z. Phys. B* **64**, 189-193 (1986).
2. Gao, L., et al. Superconductivity up to 164 K in  $\text{HgBa}_2\text{Ca}_{m-1}\text{Cu}_m\text{O}_{2m+2+\delta}$  ( $m=1, 2$ ,

- and 3) under quasi hydrostatic pressures. *Phys. Rev. B* **50**, 4260-4263 (1994).
3. Kamihara, Y., Watanabe, T., Hirano, M., & Hosono, H. Iron-based layered superconductor  $\text{La}[\text{O}_{1-x}\text{F}_x]\text{FeAs}$  ( $x = 0.05-0.12$ ) with  $T_c = 26$  K. *J. Am. Chem. Soc.* **130**, 3296-3297 (2008).
  4. Ren, Z. A., et al. Superconductivity at 55 K in iron-based F-doped layered quaternary compound  $\text{Sm}[\text{O}_{1-x}\text{F}_x]\text{FeAs}$ . *Chinese Phys. Lett.* **82**, 2215-2216 (2008).
  5. Guo, J. G., et al. Superconductivity in the iron selenide  $\text{K}_x\text{Fe}_2\text{Se}_2$  ( $0 \leq x \leq 1.0$ ). *Phys. Rev. B* **82**, 18 (2010).
  6. Kotliar, G., & Vollhardt, D. Strongly correlated materials: Insights from dynamical mean-field theory. *Phys. Today* **57**, 53-59 (2004).
  7. Qazilbash, M. M. et al. Electronic correlations in the iron pnictides. *Nature Physics* **5**, 647 (2009).
  8. Anderson, P. W. The resonating valence bond state in  $\text{La}_2\text{CuO}_4$  and superconductivity. *Science* **235**, 1196-1998 (1987).
  9. Takenaka, K., et al. Coherent-to-incoherent crossover in the optical conductivity of  $\text{La}_{2-x}\text{Sr}_x\text{CuO}_4$ : charge dynamics of a bad metal. *Phys. Rev. B* **65**, 35-42 (2002).
  10. Lee, Y. S., et al. Neutron-scattering study of spin-density wave order in the superconducting state of excess-oxygen-doped  $\text{La}_2\text{CuO}_{4+y}$ . *Phys. Rev. B* **60**, 3643-3654(1999).
  11. Takada, K., et al. Superconductivity in two-dimensional  $\text{CoO}_2$  layers. *Nature*, **34**, 53-55 (2003).
  12. Cheng, J. G., et al. Pressure induced superconductivity on the border of magnetic order in  $\text{MnP}$ . *Phys. Rev. Lett.* **114**, 117001 (2015).
  13. Wu, W., et al. Superconductivity in the vicinity of antiferromagnetic order in  $\text{CrAs}$ . *Nat. Commun.* **5**, 5508 (2014).
  14. Doan, P., et al.  $\text{Ba}_{1-x}\text{Na}_x\text{Ti}_2\text{Sb}_2\text{O}$  ( $0.0 \leq x \leq 0.33$ ): A layered titanium-based pnictide oxide superconductor. *J. Am. Chem. Soc.* **134**, 16520-165233 (2012).
  15. Takeshi, Y., et al. Superconductivity in  $\text{BaTi}_2\text{Sb}_2\text{O}$  with a  $d^1$  square lattice. *J. Phys. Soc. Jpn.* **81**, 3706 (2012).

16. Petrovic, C., et al. Heavy-fermion superconductivity in CeCoIn<sub>5</sub> at 2.3K. *J. Phys. Condens. Matter* **13**, 337 (2001).
17. Zheng, G. Q., et al. Spin singlet pairing in the superconducting state of Na<sub>x</sub>CoO<sub>2</sub>·1.3H<sub>2</sub>O: evidence from a <sup>59</sup>Co Knight shift in a single crystal. *Phys. Rev. B* **73**, 503 (2006).
18. Gavilano, J. L., et al. Unconventional charge ordering in Na<sub>0.7</sub>CoO<sub>2</sub> below 300 K. *Phys. Rev. B* **69**, 100404 (2004).
19. Haerter, J. O., Peterson, M. R., & Shastry, B. S. Strong correlations produce the Curie-Weiss phase of Na<sub>x</sub>CoO<sub>2</sub>. *Phys. Rev. Lett.* **97**, 226402 (2006).
20. Mccarthy, S. L. The superconductivity and magnetic susceptibility of some zirconium-transition-metal compounds; evidence for an anticorrelation. *J. Low Temp. Phys.* **4**, 489-501 (1971).
21. Takekuni, M., Sugita, H., & Wada, S. Nuclear-magnetic-resonance investigation of the itinerant nearly antiferromagnetic behavior in superconducting Zr<sub>2</sub>(Co<sub>1-x</sub>Ni<sub>x</sub>). *Phys. Rev. B* **58**, 11698-11702 (1998).
22. Mueller, M. H, & Knott, H. W. The crystal structures of Ti<sub>2</sub>Cu, Ti<sub>2</sub>Ni, Ti<sub>4</sub>Ni<sub>2</sub>O, and Ti<sub>4</sub>Cu<sub>2</sub>O. *Trans. Aime* **227**, (1963).
23. Rietveld, H. M. A profile refinement method for nuclear and magnetic structures. *J. Appl. Crystallogr.* **2**, 65-71 (1969).
24. Li, S., et al. Anomalous properties in the normal and superconducting states of LaRu<sub>3</sub>Si<sub>2</sub>. *Phys. Rev. B* **84**, 214527 (2011).
25. Lee, I. J., Chaikin, P. M., & Naughton, M. J. Exceeding the Pauli paramagnetic limit in the critical field of (TMTSF)<sub>2</sub>(PF)<sub>6</sub>. *Phys. Rev. B* **62**, 14669-14672 (2000).
26. Bauer, E., et al. Heavy fermion superconductivity and magnetic order in noncentrosymmetric CePt<sub>3</sub>Si. *Phys. Rev. Lett.* **92**, 027003 (2004).
27. Yuan, H. Q., et al. S-wave spin-triplet order in superconductors without inversion symmetry: Li<sub>2</sub>Pd<sub>3</sub>B and Li<sub>2</sub>Pt<sub>3</sub>B. *Phys. Rev. Lett.* **97**, 017006 (2006).
28. Wilson, K. G. The renormalization group: critical phenomena and the Kondo problem. *Rev. Mod. Phys.* **47**, 773-840 (1975).

29. Mooij, J. H. Electrical conduction in concentrated disordered transition metal alloys. *Phys. Status Solidi* **17**, 521-530 (1973).
30. Arnason, S. B., Herschfield, S. P., & Hebard, A. F. Bad Metals made with good-metal components. *Phys. Rev. Lett.* **81**, 3936-3939 (1998).
31. Mikheev, E., et al. Tuning bad metal and non-Fermi liquid behavior in a Mott material: rare-earth nickelate thin films. *Sci. Adv.* **1**, (2015).
32. Cho, K., et al. Anisotropic upper critical field and a possible Fulde-Ferrel-Larkin-Ovchinnikov state in a stoichiometric pnictide superconductor LiFeAs. *Phys. Rev. B* **83**, 407-414 (2011).
33. Mao, H. K., Xu, J., & Bell, P. M. Calibration of the ruby pressure gauge to 800 kbar under quasi-hydrostatic conditions. *J. Geophys. Res. Solid Earth* **91**, 4673-4676 (1986).



## Figures and legends

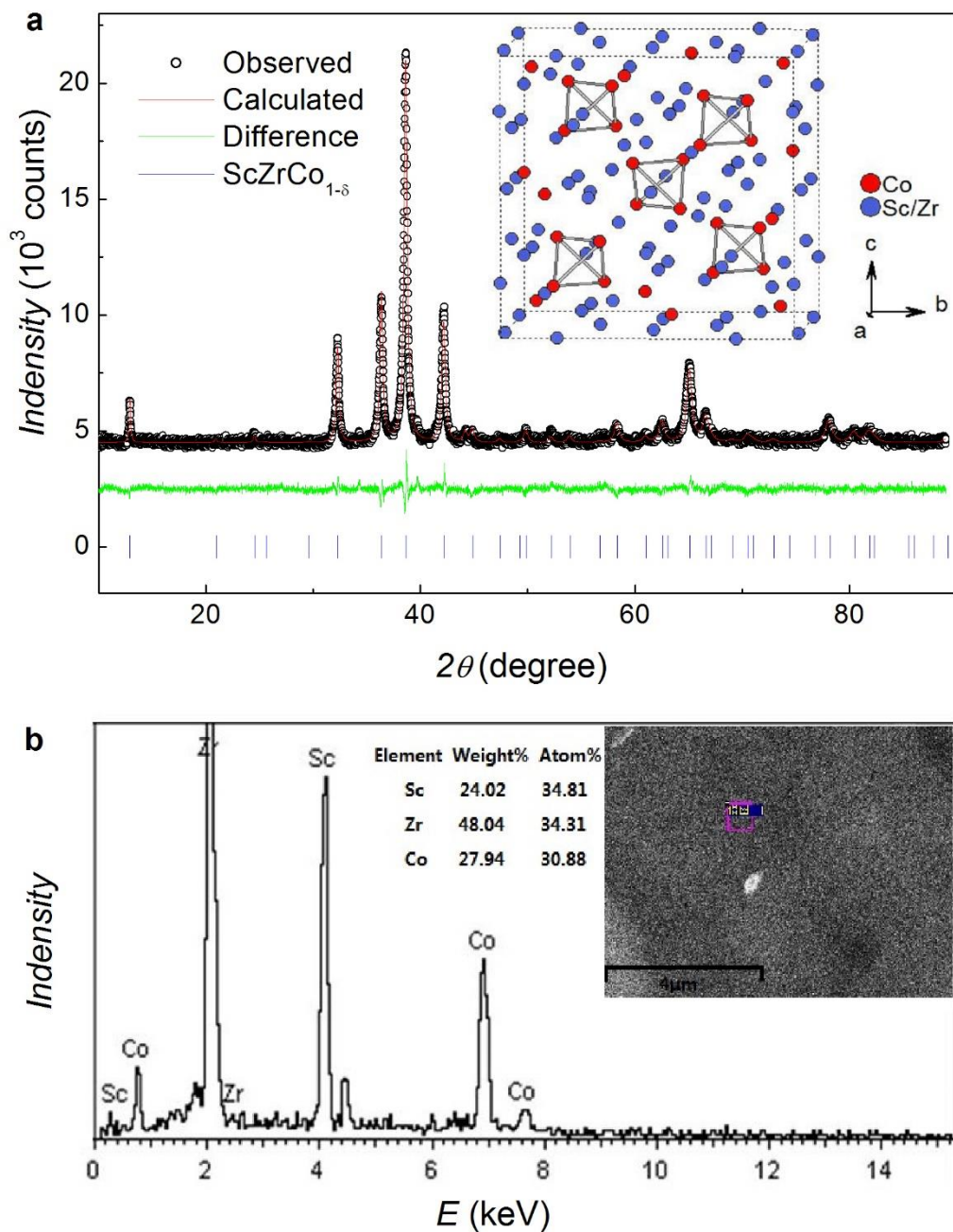


**Figure 1: The XRD and EDS patterns of ScZrCo<sub>1-δ</sub> polycrystalline. (a)** X-ray diffraction patterns and Rietveld fit for the ScZrCo<sub>1-δ</sub> polycrystalline sample. The inset shows the schematic structure. **(b)** Energy dispersive X-ray microanalysis spectrum taken on a ScZrCo<sub>1-δ</sub> polycrystalline. The inset shows the SEM photograph of the sample on which we detect the element composition of the purple line marked area.

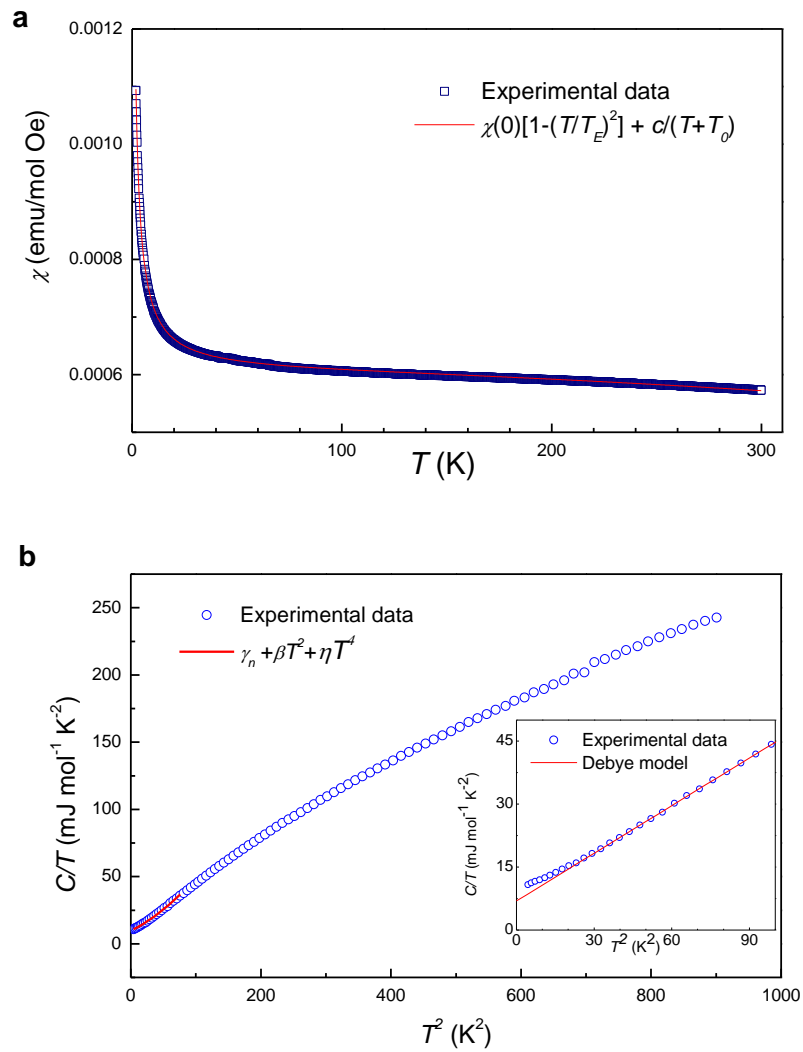


**Figure 2: Magnetic susceptibility and specific heat at ambient pressure. (a)** Temperature dependence of the magnetic susceptibility measured at 1 T. The red line is the fitting curve by the Curie-Weiss law. **(b)** The raw data of specific heat coefficient  $C/T$  vs.  $T^2$ , together with the fitting curve (red line) in the low temperature region. The inset shows the detail of the low temperature region. The red line in the inset presents the Debye model fit, an up-turning of  $C/T$  is clearly observed.

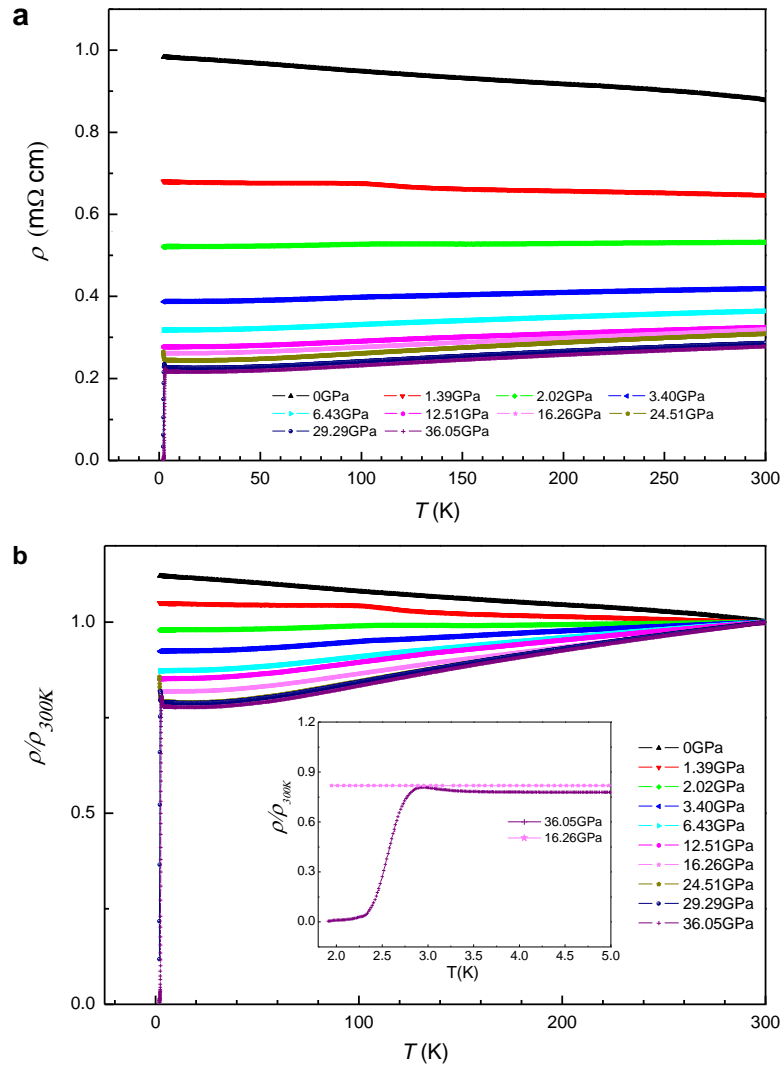


**Figure 3: Temperature dependence of resistivity in ScZrCo<sub>1-δ</sub> at high pressure. (a)**

Temperature dependence of resistivity for the sample ScZrCo<sub>1-δ</sub> in the temperature region from 1.9 K to 300 K at various pressures. **(b)** The normalized resistivity as a function of temperature at various pressures. The inset figure shows the enlarged view of comparison between two curves of resistivity versus temperature with and without superconductivity.

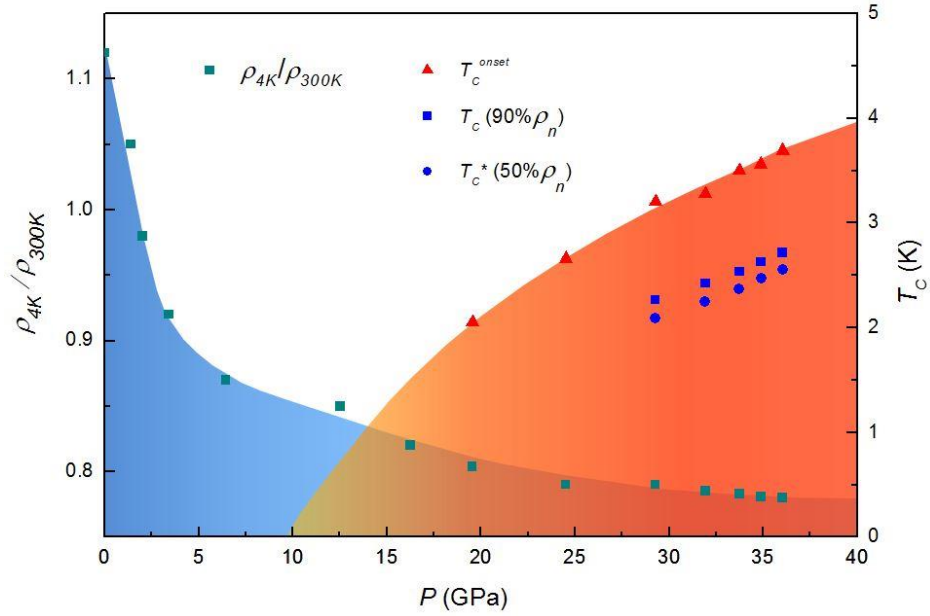


**Figure 4: Phases diagram of ScZrCo<sub>1-δ</sub>.** Pressure dependence of critical transition temperature  $T_c$  and  $\rho(4K)/\rho(300K)$  for ScZrCo<sub>1-δ</sub>. The critical transition temperature is determined by  $T_c^{onset}$  (filled red triangles), 90% $\rho_n$  (filled blue squares) and 50% $\rho_n$  (filled blue circles), respectively. The data at 19.54 GPa, 31.95 GPa, 33.76 GPa and 34.9 GPa are not shown in Fig. 3 for clarity. Instead, these data are presented in the Supplementary Information.

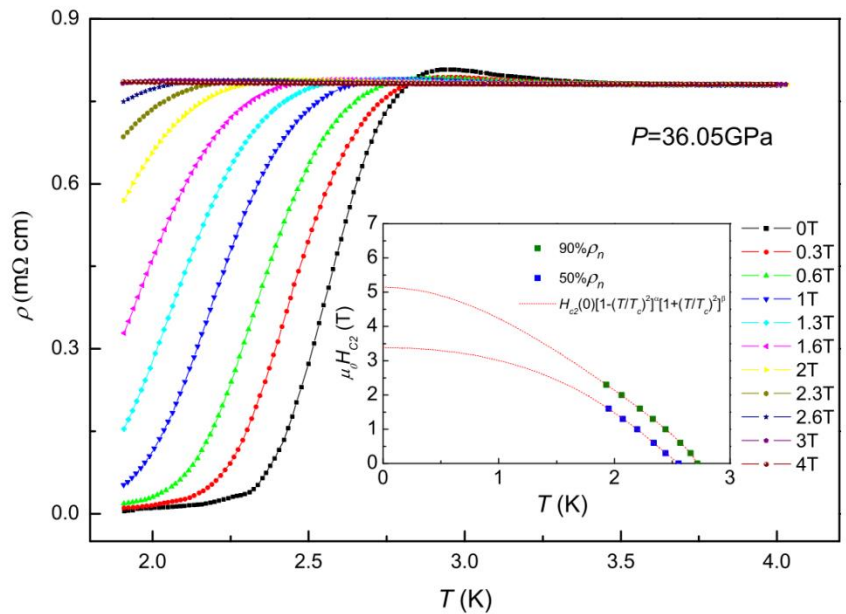


**Figure 5: Resistivity versus temperature under 36.05 GPa and upper critical field.**

Temperature dependence of resistivity for the sample  $\text{ScZrCo}_{1-\delta}$  under the pressure of 36.05 GPa in the temperature region from 1.9 K to 4 K at various magnetic fields. The inset shows the upper critical field  $H_{c2}(T)$  determined by the criterions of  $90\%\rho_n$  and  $50\%\rho_n$ , and the fitting curves (see text).

**Table 1: Crystallographic Data of  $\text{ScZrCo}_{1-\delta}$  at 300 K.**

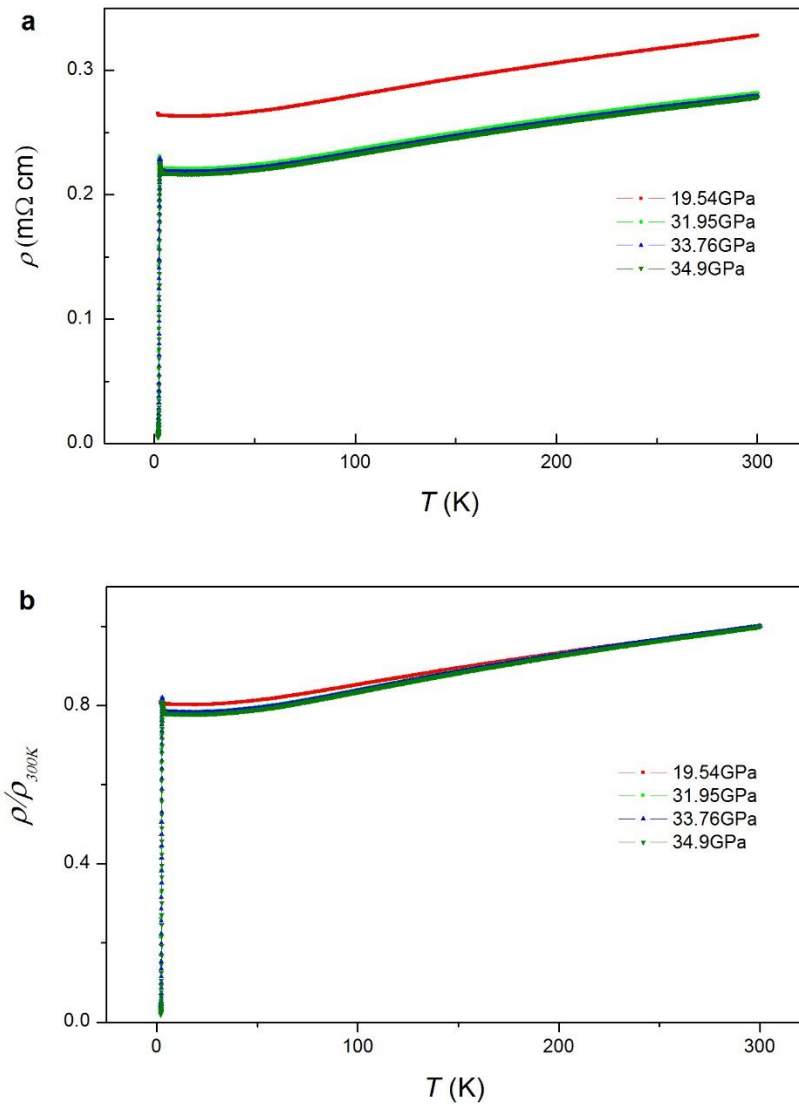
compounds		$\text{ScZrCo}_{1-\delta}$			
space group		$FD3 - MS$			
$a$ (Å)		12.2247(9)			
$V$ (Å <sup>3</sup> )		1826.939(7)			
$R_{wp}$ (%)		1.551			
atom	site	occupancy	x	y	z
Co	32e	1	0.912	0.912	0.912
Sc1	16d	0.5222	0.3099	0	0
Zr1	16d	0.4778	0.3099	0	0
Sc2	48f	0.4334	0.125	0.125	0.125
Zr2	48f	0.5666	0.125	0.125	0.125

**Supplementary Information for**

**Pressure Induced Superconductivity in the New Compound  $\text{ScZrCo}_{1-\delta}$**

Enyu Wang\*, Jing Si\*, Xiyu Zhu†, Guan-Yu Chen, Hai Lin & Hai-Hu Went

1. Temperature dependence of resistivity at various pressures. For clarity, these data are not shown in the main text.



**Supplementary Figure 1: Temperature dependence of resistivity in ScZrCo<sub>1.6</sub> at various pressures.** (a) Temperature dependence of resistivity for the sample ScZrCo<sub>1.6</sub> in the temperature region from 1.9 K to 300 K at various pressures. (b) The normalized resistivity  $\rho(T)/\rho_{300K}$  as a function of temperature at various pressures.